Bulletin of the Seismological Society of America, Vol. 103, No. 2A, pp. 1022–1037, April 2013, doi: 10.1785/0120120024

Ⓔ

Refining the Southern Extent of the 1872 Owens Valley Earthquake Rupture through Paleoseismic Investigations in the Haiwee Area, Southeastern California

by Colin B. Amos, Andrew T. Lutz, Angela S. Jayko, Shannon A. Mahan, G. Burch Fisher, and Jeffrey R. Unruh

Abstract Recent upward revision of the 1872 Owens Valley earthquake from M_w 7.4–7.5 to 7.7–7.9 implies either additional unrecognized rupture length or anomalously strong ground motions associated with this event. We investigate the first possibility through paleoseismic trenching south of the mapped surface rupture in the Haiwee area, where historical accounts suggest significant surface deformation following the earthquake. Trenching focused on a prominent north-striking scarp, herein termed the Sage Flat fault, expressed in Pleistocene alluvial fans east of Haiwee Reservoir. Surficial mapping and ground-based Light Detection and Ranging (lidar) surveying suggest that this fault accommodates east-down normal motion, and possibly a comparable amount of dextral slip. Trenching and luminescence dating brackets the timing of the most recent surface-rupturing earthquake between ~25.7 and 30.1 ka, and provides evidence for an earlier event predating this time. In combination with scarp profiling, these dates also suggest a maximum rate of normal, dip-slip fault motion up to ~0.1 mm/yr over this period. Although we discovered no evidence for recent surface rupture on the Sage Flat fault, a series of subvertical fractures and fissures cut across young trench stratigraphy, consistent with secondary deformation associated with seismic shaking. As such, we suggest that possible ground disturbance in the Haiwee area during the 1872 event primarily reflected ground shaking or liquefaction-related deformation rather than triggered slip. In addition, we infer a structural and kinematic connection between the Owens Valley fault and oblique-dextral faults north of Lower Cactus Flat in the northwestern Coso Range, rather than a west-step into northern or western Rose Valley. Consideration of these structures in the total extent of the Owens Valley fault suggests a length of 140 km, of which at least 113 km ruptured during the 1872 event.

Online Material: Procedural details and expanded results from the OSL sample analyses, as well as high-resolution paleoseismic trench logs.

Introduction

Source parameters for large historical earthquakes provide critical constraints on empirical relationships used in seismic hazard assessments (e.g., Wells and Coppersmith, 1994). Such assessments rely on both geological and seismological observations of past earthquakes to evaluate the potential location and frequency of future earthquake ruptures. In areas dominated by distributed intracontinental strain, historical surface ruptures commonly exhibit complex surface deformation patterns, including offset along multiple and discontinuous fault strands during a single event. Two recent historical events in eastern California, the 1992 Landers and 1872 Owens Valley earthquakes, produced relatively segmented surface ruptures that would arguably not have been identified as single throughgoing fault structures prior to the seismic events (Hough and Hutton, 2008). In each case, the complex and discontinuous nature of these surface ruptures reflects in some part a combination of relatively low average slip rate and long recurrence intervals for both faults (e.g., Rockwell *et al.*, 2000; Bacon and Pezzopane, 2007). Therefore, documentation of segmented surface ruptures or local triggered slip provides additional constraints on the hazards posed by large but infrequent earthquakes on faults distant from major plate boundaries.

The recent and provocative suggestion that the 1872 Owens Valley earthquake magnitude be revised upwards to M_w 7.7–7.9 (compare dePolo *et al.*, 1991; Hough and

Hutton, 2008) suggests that faults in the eastern California are capable of earthquake magnitudes rivaling the largest historical San Andreas events (compare Hanks and Kanamori, 1979). The Hough and Hutton (2008) recent magnitude estimate relies on reinterpretation of macroseismic observations of shaking intensities during the 1872 event, which were more widely felt than the 1906 San Andreas earthquake. Given uncertainty in the total extent of the Owens Valley surface rupture, reflecting in part the segmented nature of the fault zone (Fig. 1), Hough and Hutton (2008) explain this discrepancy by suggesting that (1) either the area of the 1872 rupture was greater than currently recognized or (2) the Owens Valley earthquake produced systematically higher ground motions over regional distances. Several historical accounts of surface deformation beyond the limits of the recognized 1872 rupture bolster the first possibility (e.g., Whitney, 1872a,b). The second interpretation raises the important possibility that low-slip-rate faults away from the San Andreas plate boundary might produce a fundamentally different class of earthquake (compare Hecker *et al.*, 2010), and importantly, that other such 100–140-km-long faults in California could be capable of similar large-magnitude events.

Here, we present the results from paleoseismic trenching at Sage Flat, south of the Owens Valley fault, to test whether the revised magnitude estimate can be attributed to additional surface rupture south of the mapped fault trace (Fig. 1). We logged three excavations across a fault scarp cutting upper Pleistocene alluvium near Haiwee Reservoir, where accounts by Whitney (1872a,b) months after the earthquake suggest the presence of youthful scarps and significant ground deformation. The trenched scarp, herein referred to as the Sage Flat fault, traverses a relatively broad alluvial piedmont at the base of the eastern Sierra Nevada (Fig. 1). Although the roughly north-striking Sage Flat fault is discontinuous with the north-northwest trending Owens Valley fault, recent work in the area documents triggered slip during the 1872 earthquake on a similarly oriented fault cutting the northern Coso Range piedmont (Slemmons *et al.*, 2008). Accordingly, we seek to document the timing of past earthquakes on the Sage Flat fault to test for fault segmentation or triggered slip during the 1872 event. We also present surficial geologic mapping, luminescence dating, and results from a ground-based Light Detection and Ranging (lidar) survey to constrain the orientation, timing, and slip rate on the Sage Flat fault. Our results limit the southwestern extent of the southern Owens Valley fault and place additional constraints on the spatial extent of the 1872 surface rupture.

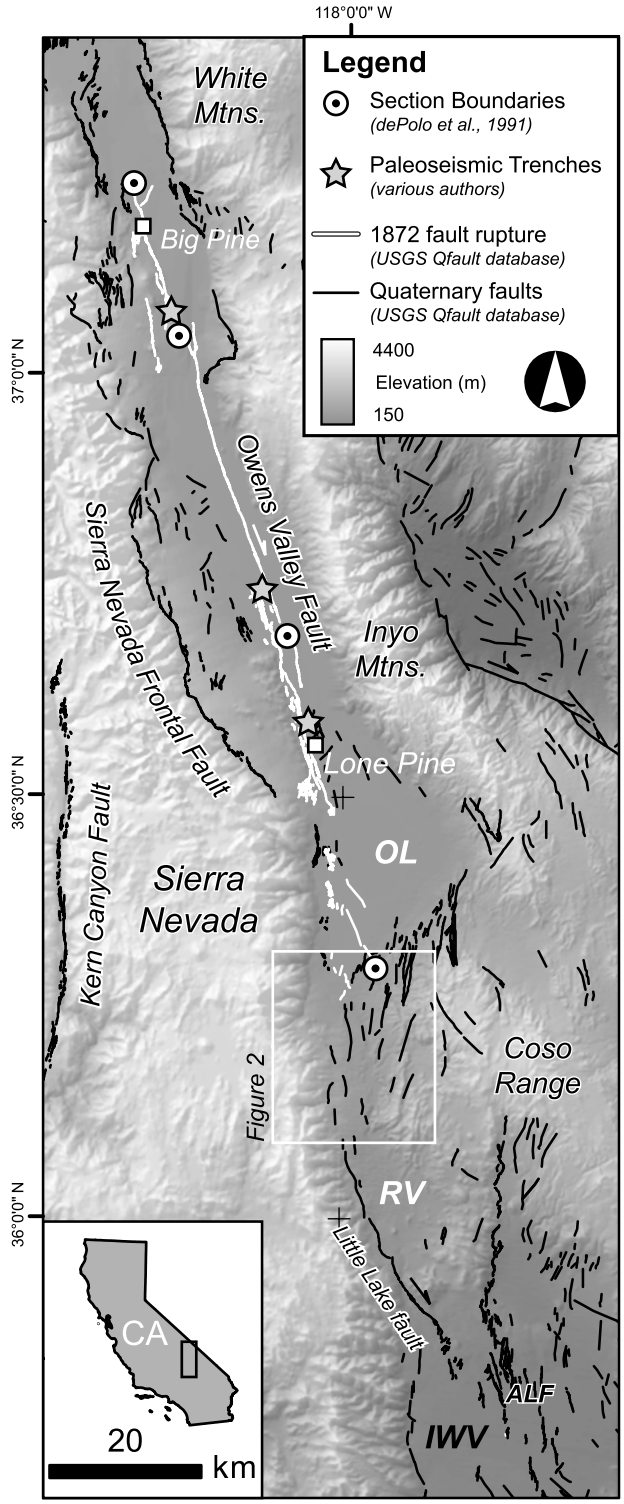

Figure 1. Regional overview of the Owens Valley fault and the 1872 earthquake surface rupture, showing the location of previous paleoseismic trenches and fault section boundaries from dePolo *et al.* (1991). Fault traces are taken from the U.S. Geological Survey's Quaternary Fault and Fold Database (USGS and California Geological Survey; see Data and Resources) with the exception of the Kern Canyon fault (Brossy *et al.*, 2012). ALF, Airport Lake fault; OL, Owens Lake; RV, Rose Valley; IWV, Indian Wells Valley.

Background and Previous Work

The Owens Valley Fault

The Owens Valley fault is part of a broad, distributed network of active strike-slip and normal faults east of the Sierra Nevada in California (Fig. 1). Collectively termed

the eastern California seismic belt (Wallace, 1984), the eastern California shear zone (Dokka and Travis, 1990) or Walker Lane belt (e.g., Stewart, 1988; Wesnousky, 2005), this zone of deformation accommodates roughly one quarter (9 ± 2 mm/yr) of the total dextral motion between the Pacific and North American plates (Bennett *et al.*, 2003). Of the total displacement, the Owens Valley fault accounts for approximately 1–4.5 mm/yr of dextral slip (Beanland and Clark, 1994; Lee *et al.*, 2001; Bacon *et al.*, 2003; Bacon and Pezzopane, 2007; Kirby *et al.*, 2008), averaged over the late Pleistocene to Holocene. Most estimates of fault slip-rate from geologic features fall at the lower end of that range, in overall agreement with, albeit slightly lower than, rate estimates derived from Global Positioning System data (2.1 ± 0.7 mm/yr, Dixon *et al.*, 2003).

The 26 March 1872 earthquake ruptured a distance of at least 113 km along the Owens Valley fault (Fig. 1), from north of Big Pine to the southern shoreline of the now-dry Owens Lake (Slemmons *et al.*, 2008). Although sparsely populated at the time, the earthquake caused approximately 27 fatalities in the nearby settlement of Lone Pine (Whitney, 1872a) and created strong ground motions felt over much of California (Oakeshott *et al.*, 1972; Stover and Coffman, 1993; Hough and Hutton, 2008). Initial field assessments of the damage extent and observations of surface deformation are presented by Whitney (1872a,b). Subsequent descriptions and observations in the following decades, including those by G. K. Gilbert in 1884, are summarized by Beanland and Clark (1994), Hough and Hutton (2008), and Slemmons *et al.* (2008). Nearly a century later, D. B. Slemmons, summarized in Hill (1972), carried out the first modern, systematic mapping of the Owens Valley fault and the 1872 rupture using low-sun-angle aerial photography. Carver (1969) also mapped the southern Owens Valley fault zone, focusing on deformation south of Diaz Lake around the margin of the dry Owens Lake. Notably, this work made the important distinction between surface deformation related to slip on faults and that caused by shaking-induced lateral spreading and liquefaction, particularly focused around the latest Pleistocene to early Holocene shorelines.

Subsequent published mapping of the Owens Valley fault documents the relatively complex surface trace of the 1872 rupture (Fig. 1), which included slip on numerous secondary fault strands and subparallel-to-oblique fault splays (D. B. Slemmons, summarized in Hill (1972); Beanland and Clark, 1994; Slemmons *et al.*, 2008). These discontinuities suggest division of the fault into several geometric sections based on the presence of fault stepovers, splays, or changes in the overall fault strike (Fig. 1; dePolo *et al.*, 1991). Lateral offset from the 1872 surface rupture averaged 6 ± 2 m, although the maximum lateral offset (10 m) occurred at the southern end of the fault near Lone Pine (Beanland and Clark, 1994). Compilation of fault offsets from the 1872 event along the length of the Owens Valley fault indicates that right-lateral offset dominated during the 1872 event and occurred at an average ratio of 6:1 relative to subordinate east-down normal motion (Beanland and Clark, 1994).

Previous paleoseismic trench studies along the Owens Valley fault (Fig. 1) reveal evidence for additional paleoearthquakes on segments that ruptured during the 1872 event. The penultimate event identified by Lee *et al.* (2001) near Big Pine occurred between 3 and 4 ka. Evidence for this earthquake is absent in fault trenches near Lone Pine, however, and Bacon and Pezzopane (2007) attribute this event to triggered slip caused by rupture on the nearby White Mountain frontal fault (Fig. 1). The penultimate rupture identified by Bacon and Pezzopane (2007) near Lone Pine occurred between 8.8 and 10.2 ka, consistent with recurrence intervals estimated by Lubetkin and Clark (1988) and Bierman *et al.* (1995). Bacon and Pezzopane (2007) also provide evidence for an antepenultimate event sometime between 15 and 25 ka, yielding an average recurrence interval of roughly 10 k.y. or greater for the Owens Valley fault.

Extent of the 1872 Earthquake Rupture

Considerable uncertainty surrounds published estimates of the total length of the Owens Valley fault and the 1872 surface rupture. This uncertainty reflects a number of factors, including the discontinuous nature of surface faulting and complexities in the fault surface trace. Additionally, vagueness and variability in historical descriptions of surface deformation, in part because of confusion between surface faulting and fissures or shaking-related deformation, confounds the true length of the surface rupture. The U.S. Geological Survey Quaternary Fault and Fold Database (USGS and California Geological Survey; see Data and Resources) lists the 1872 rupture section of the Owens Valley fault as spanning 118 km of a total 136-km fault length. This total length includes fault scarps north of Big Pine abutting the Sierra Nevada range front (Fig. 1), extending north toward Bishop. Historical accounts from J. D. Whitney, quoted and paraphrased in several sources (Hobbs, 1910; Bateman, 1961; Slemmons *et al.*, 2008), suggest pervasive ground cracking between Bishop and Big Pine, although most studies limit the 1872 rupture termination immediately north of Big Pine (Beanland and Clark, 1994; Slemmons *et al.*, 2008).

The southern shore of Owens dry lake represents the currently accepted southern termination of the Owens Valley fault and the 1872 surface rupture (Slemmons *et al.*, 2008; Fig. 2). Offset historical shorelines identified by Slemmons, and later surveyed by Vittori *et al.* (1993) indicate 1.8–2.3 m of right-lateral offset during the 1872 earthquake. Recognition of these offset shorelines extends the earlier rupture mapping of Beanland and Clark (1994) by ~20 km to the southeast. Slemmons *et al.* (2008) also describe evidence for recent faulting south of the historical shoreline mapped by Carver (1969), including north-striking normal fault scarps flanking a series of low volcanic hills on the northern Coso piedmont (Red Ridge fault of Vittori *et al.*, 1993; Fig. 2). Inclusion of faulting at Red Ridge, presumably

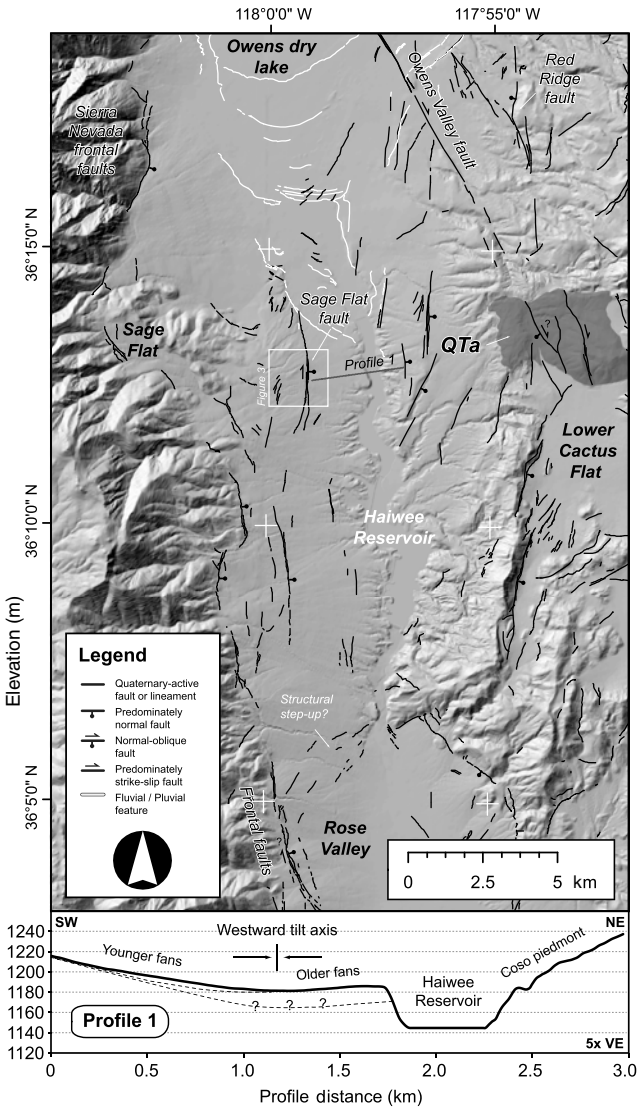

Figure 2. Hillshade image showing the Sage Flat fault and other Quaternary active structures in the Haiwee area. Fault mapping is modified after Jayko (2009). QTa refers to a Plio-Quaternary andesite flow cut by a series of faults along-strike of the Owens Valley fault. Inset shows a topographic profile extracted from the NED 10-m digital topography across the Sage Flat piedmont and Haiwee Reservoir. See text for discussion.

triggered during the 1872 earthquake, suggests a total rupture length of at least 113–120 km.

Several additional lines of evidence leave open the possibility of fault-related surface deformation south of the currently recognized 1872 rupture termination (Hough and Hutton, 2008). First, historical accounts from J. D. Whitney indicate pervasive ground cracking and differential settling in the vicinity of Haiwee Meadows, which coincides with the former spillway channel between latest Pleistocene Owens Lake and the Owens River (Bacon *et al.*, 2006) now occupied by Haiwee Reservoir (Fig. 2). Along the margin of Haiwee Meadows, Whitney (1872a) attributed a youthful scarp near to the 1872 event. Although his description predates understanding of the specific connection between faulting and earthquakes, or the distinction between fault slip and lateral spreading, Whitney hints at a dependence of these features on groundwater and their position along the meadow (also quoted in Hough and Hutton, 2008; Slemmons *et al.*, 2008):

> "The dependence of the fissures upon the character of the soil was well exemplified at Haiwee Meadows, which occupy an oval area somewhat less than a mile in diameter, surrounded by hills, all around the border of which the soil is wet and heavy, owing to the presence of numerous springs in that position. Along this border the ground is broken by fissures, and the inside edge has settled as much as four or five feet. The hills to the east of the meadows are of volcanic sediment; and on visiting them a large crack was observed running in an easterly direction across one of the spurs, which looked fresh, as if it might have been made during the recent earthquake."

Indirect evidence for continuation of the 1872 surface rupture beyond its recognized boundaries comes from an apparent gap in microseismicity spanning the length of the Owens Valley into the Haiwee area (Hough and Hutton, 2008). This gap also extends northward into the area where Whitney (1872a) described pervasive ground deformation associated with the 1872 earthquake. Hough and Hutton (2008) note that, although not conclusively linked with the 1872 surface rupture, low overall rates of background seismicity span a length of 140 km, similar to the total extent of the Owens Valley fault.

To test whether or not surface faulting during the 1872 event extended onto structures near the former Haiwee Meadows, we completed an investigation of a previously unstudied fault at Sage Flat (Fig. 2). This site was selected based on the prominent geomorphic expression of the Sage Flat fault in comparison with other nearby structures and the locally steep scarp face, which implies a lesser degree of erosion and diffusion for this portion of the scarp. Additionally, the presence of finer-grained subsurface materials ponded against the Sage Flat fault provides a favorable target for trenching relative to the coarse alluvium forming the surrounding bajada. In the following sections, we present new constraints on surface ruptures on the Sage Flat fault and discuss potential kinematic and structural linkages with the Owens Valley fault.

Study Area

Neotectonic Setting of the Haiwee Area, Southern Owens Valley

The Haiwee area lies in the southernmost Owens Valley (Figs. 1 and 2) and occupies the north flank of a topographic divide that intermittently served as a spillway between Pleistocene glacial lakes in Owens and Rose Valleys. Incision of the Pleistocene Owens River channel through coalescing

alluvial fans that underlie this divide attests to regional tectonic lowering of valley floors between Owens in the north and Searles Valley in the southeast. A series of small, northeast-striking scarps mapped by Jayko (2009) (Fig. 2) indicate that the ~200 m topographic drop between Haiwee Reservoir and Rose Valley to the south may be structurally controlled.

Surface deformation east and northeast of the Sage Flat paleoseismic site records transfer of dextral shear from the Owens Valley fault system southward into the northern Coso Range via a series of small pull-apart basins (e.g., Lower Cactus Flat; Fig. 2) and horst blocks bounded by right-lateral strike-slip, normal, and oblique slip faults (Jayko, 2009). The extensional relay system continues southward and links to the dextral Little Lake and Airport Lake faults, which define an overall releasing stepover across the southern Coso Range (Unruh *et al.*, 2002; Fig. 1). The Sage Flat paleoseismic site is situated in a transition zone between the normal or oblique-normal Sierra Nevada Range front system and the dextral Owens Valley fault zone (Fig. 2).

Quaternary structures in the northwestern Coso Range east of Haiwee Reservoir include a series of discontinuous, north-northwest-striking normal and oblique normal faults, a broad tilt panel of west-dipping Plio-Quaternary cover sediments, and fault-related folds that deform clastic and volcanic deposits of the Plio-Pleistocene Coso Formation (Stinson, 1977; Duffield and Bacon, 1981; Jayko, 2009). Although no throughgoing structures directly connect to the Owens Valley fault to the north, several similarly oriented faults cut the surface of a Plio-Quaternary andesite (QTa; Fig. 2) at the northern end of Lower Cactus Flat. Frankel *et al.* (2008) discuss evidence for dextral displacement along these structures. The easternmost of these faults is expressed as a series of alternately east- and west-facing scarps and apparent shutter ridges that bound isolated pockets of Quaternary alluvium. Evidence for dextral displacement along the western fault strand is less well constrained (Duffield and Bacon [1981] map it as a normal fault), although we note an apparent right-lateral separation for both structures where they intersect the northern, eroded contact between andesite and the underlying Coso Formation and basement rocks. To the south, both faults terminate into a series of northeast-striking, en echelon normal faults bounding the western edge of Lower Cactus Flat (Jayko, 2009). We infer that, together, active faults at Lower Cactus Flat represent the northern end of an extensional relay linked the southern part of the Owens Valley fault zone.

Structures in the Haiwee area west of Lower Cactus Flat consist of a relatively discontinuous series of north-striking faults between the Sierra Nevada range front to the west and the Coso piedmont to the east (Fig. 2). These faults display predominately east-down normal offsets and may accommodate some degree of westward tilting of the Haiwee block west of Lower Cactus Flat. The Sage Flat fault represents one of these east-down normal structures at the northern end of the Haiwee area.

Surficial Geology of Sage Flat

Sage Flat refers to the small, nearly closed depression southwest of Owens Lake (Fig. 2), where an isolated bedrock block interrupts the generally eastward flow of alluvial fans draining the steep eastern Sierra Nevada escarpment. Alluvial fans at Sage Flat are diverted around the southern tip of this block before merging with the east-sloping bajada at the southern end of Owens Valley. Across this bajada, several generations of Pleistocene and Holocene alluvial fans coalesce and are actively incised by small creeks and washes draining toward Haiwee Reservoir, which inundates the Pleistocene Owens River spillway channel (Bacon *et al.*, 2006) and the former Haiwee Meadows (Fig. 2). Surficial geologic mapping modified after Jayko (2009) suggests at least four generations of fan deposits at Sage Flat, including active alluvial washes (Fig. 3). The eastward slope of older Pleistocene alluvial fans at Sage Flat is locally interrupted by a narrow zone of apparent westward tilting about an axis oriented parallel to the shore of Haiwee Reservoir (Fig. 2). Younger fan deposits are graded to this low, where the modern valley axis is offset to the west from the former spillway channel to the east (Jayko, 2009).

Pleistocene alluvial fans at Sage Flat comprise boulders, cobbles, and sand sourced from steep mountainous catchments fringing the eastern Sierra escarpment (Figs. 1 and 2). Construction of these fans reflects deposition of coarse debris-flows onto the piedmont surface and subsequent incision and reworking during runoff events (Whipple and Dunne, 1992). Incision and channelization isolates and stabilizes older fans and results in progressive soil formation on alluvial fan surfaces. Although numerical dates on fan surfaces at Sage Flat are unavailable, the morphostratigraphic position of these surfaces, as well as varying surface roughness and dissection provides clues as to their relative ages. For simplicity, we follow the unit classification of Jayko (2009) and group surfaces into older (Qfo), intermediate (Qfi), younger (Qfy), and active alluvial fans (Qaw). We emphasize, however, that these classifications for the undated fans at Sage Flat represent only a loose correlation and likely encompass significant age variation within each category. Cosmogenic exposure dating of alluvial fan boulders on similar surfaces in the Owens Valley piedmont yield predominately Late Pleistocene and younger ages (Bierman *et al.*, 1995; Zehfuss *et al.*, 2001; Benn *et al.*, 2006; Duhnforth *et al.*, 2007; Le *et al.*, 2007), most likely reflecting an upper bound on the preservation of intact alluvial fan boulders in this area.

The study site at Sage Flat occupies a small, localized depression between coalescing lobes of intermediate-age alluvial fans (Qfi) incised into older fan deposits (Qfo) (Fig. 3). Seepage or groundwater discharge occurs along the scarp and results in trapping of fine-grained clastic deposits near its base. A patchy cover of eolian sand and silt capping older fan deposits is preserved west of the scarp, on the upthrown side. As discussed in the following sections, these cover

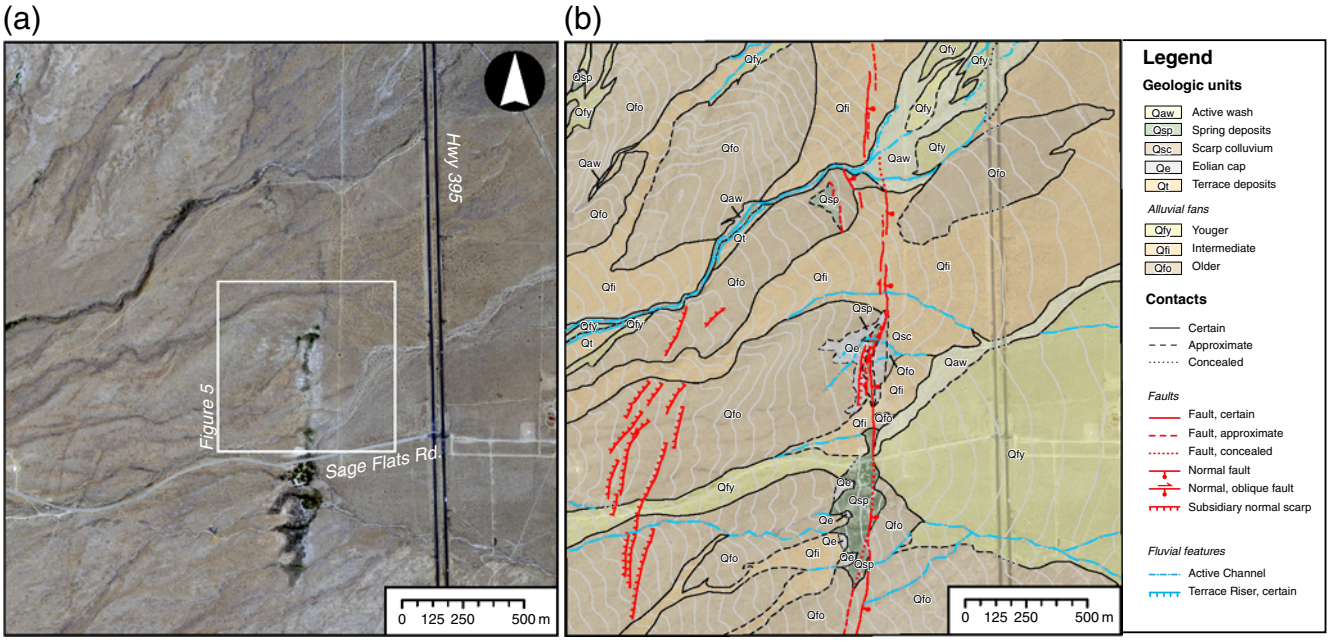

Figure 3. (a) 2009 NAIP image showing the Sage Flat site. (b) Surficial geologic map of the Sage Flat trench site, modified after Jayko (2009). The color version of this figure is available only in the electronic edition.

sediments may represent loess deposited during periods of Owens Lake desiccation in the Late Pleistocene.

Quaternary Faulting at Sage Flat

An arcuate, east-facing scarp traverses the Sage Flat piedmont for roughly 7 km, immediately south of Owens dry lake (Fig. 2). This scarp, informally termed the Sage Flat fault in this report, is one of several discontinuous north-striking faults expressed in Pleistocene alluvial fans west of Haiwee Reservoir. These faults are identified as cutting Quaternary alluvial materials in the regional geologic mapping of Stinson (1977) and Duffield and Bacon (1981). Subsequent mapping of these structures by Wills (1989) and Jayko (2009) suggests that multiple generations of Pleistocene alluvial fans are cut by the Sage Flat fault, indicating several surface ruptures over this period. The greatest relief on the Sage Flat fault (~8 m) is located at its northern end, where the scarp has been modified by fluvial erosion along the margin of a spillway channel or by wave energy along a Pleistocene erosional shoreline of Owens Lake.

Detailed mapping of the Haiwee piedmont faults, termed the Haiwee section of the Sierra Nevada fault zone by Wills (1989), indicates subtle evidence for some component of right-lateral displacement in addition to east-down normal motion on these faults. In addition to laterally deflected drainages along range front faults farther south in Rose Valley (Fig. 1), Wills (1989) suggested that the left-stepping, en echelon pattern of subtle, west-facing scarps just west of the Sage Flat fault (Fig. 3) reflects an overall right-oblique sense of displacement. Field inspection of ephemeral channels crossing the Sage Flat fault (Fig. 4) also reveals lateral deflection of these drainages on the order of 1–3 m, supporting the notion that this scarp accommodates some component of right-oblique normal motion. If so, generally north-striking fault segments to the north and south of the trench site define a slight releasing stepover (Fig. 3).

The compound nature of the Sage Flat fault is well illustrated by terrestrial laser scanning (TLS) of offset alluvial fans at our trench site (Fig. 5). This survey enables detailed topographic characterization of the scarp morphology and measurement of the total vertical offset across the scarp. TLS surveying utilized a RIEGL LMS-Z420i ground-based lidar system and resulted in collection of approximately 8.6 million individual laser returns at an average density of ~200 points/m^2. Non-ground returns from sparse brush covering the area were filtered using Bentley MicroStation software, and the remaining returns were gridded to create a digital elevation model (DEM) at a nominal resolution of 50 cm (Fig. 5; compare Perroy *et al.*, 2010).

DEM elevations were extracted along the main trace of the Sage Flat scarp in addition to a series of scarp-perpendicular topographic profiles (Figs. 5 and 6). The greatest scarp relief occurs along the central portion of our site where older fan deposits (Qfo) to the west are upthrown 8 m relative to isolated buried older alluvial fan deposits and infilling younger fans (Qfi) to the east (profiles E and F; Fig. 6). The relatively steep scarp face in this location (locally ~30°) reflects in part the relatively cohesive nature of the underlying spring deposits and saturated eolian cover on the upthrown side. Localized collapse of the over-steepened scarp has occurred on several subparallel east-facing scarps adjacent to our trench site (Fig. 5). Young alluvial fan deposits are continuous across the Sage Flat scarp at the northern end of

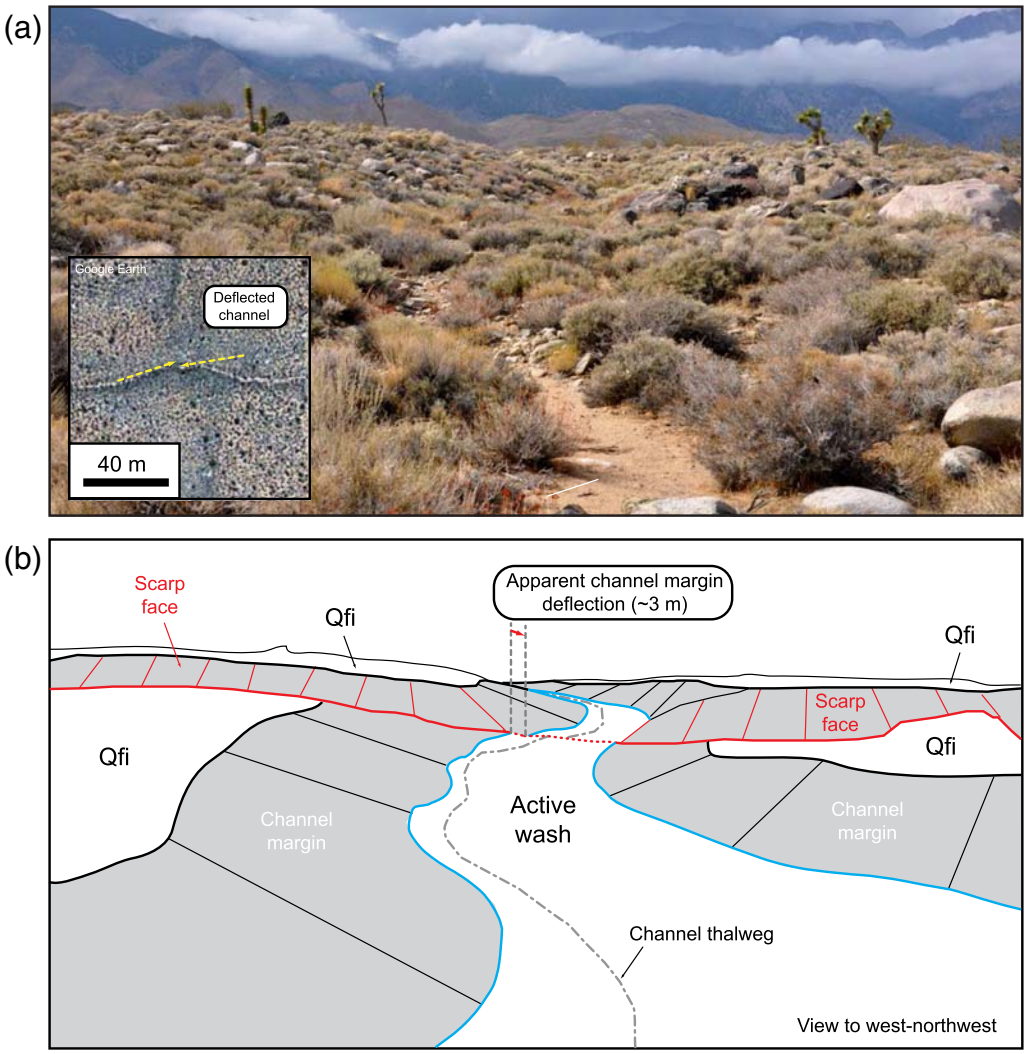

Figure 4. (a) Field photograph and (b) schematic line drawing of the Sage Flat scarp and the laterally deflected margins of an ephemeral wash intersecting the fault. Joshua trees on the scarp are ~2 m tall. Location of this vantage is shown in Figure 5. Inset in (a) shows 2009 NAIP aerial imagery of the offset channel. The color version of this figure is available only in the electronic edition.

our TLS survey, where topographic profiling suggests 2.5 ± 0.3 m of vertical separation, corresponding to a normal, dip-slip displacement of ~2.6 m on a 75° dipping fault (profile B; Fig. 6). This dip value was chosen to mimic the steeply east-dipping fault planes observed in trench exposures. The margins of an ephemeral stream channel north of our survey (Fig. 4a) show a similar magnitude of lateral deflection (~2–3 m) based on measurements made in the field (Fig. 4).

Paleoseismic Trenching at Sage Flat

Site Conditions and Investigation Methods

Paleoseismic trenching of the Sage Flat fault was conducted in October 2010 to determine the timing and size of past surface ruptures and to look for evidence of surface deformation associated with the 1872 Owens Valley earthquake. The trench site sits ~8 km south of Olancha, California, near the intersection of Sage Flats Road and U.S. Route 395. One ~20-m-long trench and two smaller 7-m-long test pits were excavated in a localized depression roughly 350 m wide (Fig. 7a), bounded on the west by a locally 8-m-high east-facing fault scarp and on the north and south by the edges of incised alluvial fans (Fig. 5).

The trench and test pits at the Sage Flat site were exposed using a track-mounted hydraulic excavator with a 36-inch-wide bucket. The south wall of each excavation was scraped clean to remove bucket smear and polish from the trench exposures. A horizontal level datum was established, and stratigraphic contacts and other features (e.g., faults) were identified and flagged using nails and colored tape. The walls of the exposures were logged at 1 inch = 1 m to depict lithology, lithologic contacts between units and subunits, and pedogenic horizons. Scaled versions of our interpretive trench logs are presented in Figure 8, and detailed versions at the original draft scale are shown in Ⓔ Plates S1 and S2 (available in the electronic supplement to the article).

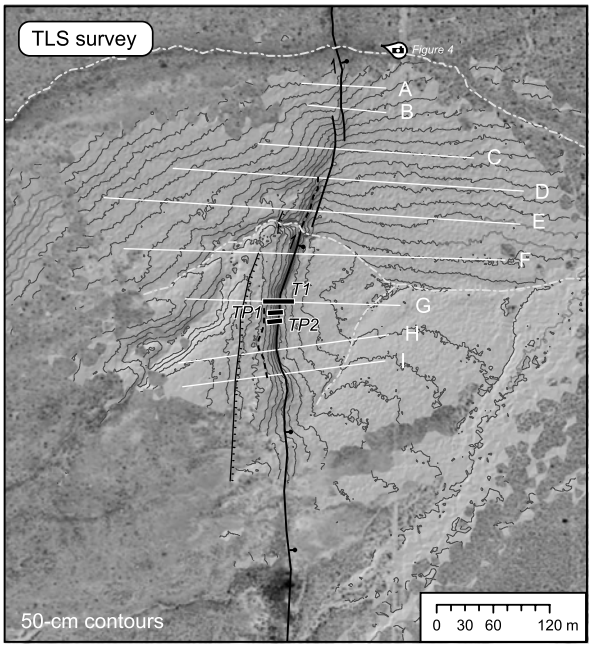

Figure 5. Hillshade image of the Sage Flat trench site created from 50-cm-resolution digital topography surveyed using a ground-based lidar. White lines correspond to the location of profiles shown in Figure 6 (T1, trench 1; TP1, test pit 1; TP2, test pit 2).

Deposits exposed in the walls of the excavations were described using the Unified Soil Classification System (American Society for Testing and Materials, ASTM, 2000). Exposed stratigraphic units were distinguished primarily based on variation in lithology, color, and relative soil profile development (e.g., color, consistency, and structure). Detailed soil profiles were described in each trench following Birkeland (1999) and Schoenberger *et al.* (2002). After completion of our study, the trench and test pits were backfilled using the original excavated materials, and the site was restored as closely as practical to original conditions.

Subsurface Geology

Subsurface materials exposed at the Sage Flat site can be grouped into three general categories, each separated by an unconformable contact: alluvial fan deposits (units 10 and 20), eolian sand (units 30, 32, 34, and 36), and scarp-derived colluvium (units 40, 50, 52, 54, 56, and 60) (Fig. 8). Stratigraphic relationships between these units are shown in detailed logs for trench T1 and test pit TP1 (Fig. 8). Shallow groundwater conditions limited the depth of trench excavations to <2 m. Groundwater is also responsible for the pervasive weathering of uncovered subsurface deposits (Fig. 7b), which obscured stratigraphic relationships and evidence for faulting in test pit TP2.

The lowest stratigraphic unit exposed at the Sage Flat site is fine- to coarse-grained sand containing gravel, cobbles, and boulders (unit 10). The western portion of this deposit is pervasively mottled with yellowish brown and dark greenish gray colors and contains abundant granitic cobbles and boulders that have weathered completely to grus. Stratification in unit 10 is indistinct because of the coarse nature of this deposit. A similar deposit (unit 20) rests stratigraphically above unit 10 at the eastern end of trench T1, and consists of yellowish brown fine- to medium-grained sand with silt and gravel, cobbles, and boulders. Unit 20 can be distinguished from unit 10 by a slightly finer-grained matrix and the presence of subhorizontal lags of flat-topped and weathered cobbles and boulders. The exact nature between units 10 and 20 is unclear, although some evidence for faulting separates these two deposits at the base of trench T1. Both units 10 and 20 represent alluvial fan deposits correlated with the older alluvial fan surface (Qfo) surrounding the trench site (Fig. 3), and may represent lateral variation within stratigraphic units of the same age.

The next oldest trench deposit, unit 30, is a light olive-brown silty clayey fine-grained sand unconformably overlying unit 10 at western end of trench T1 and test pit TP1

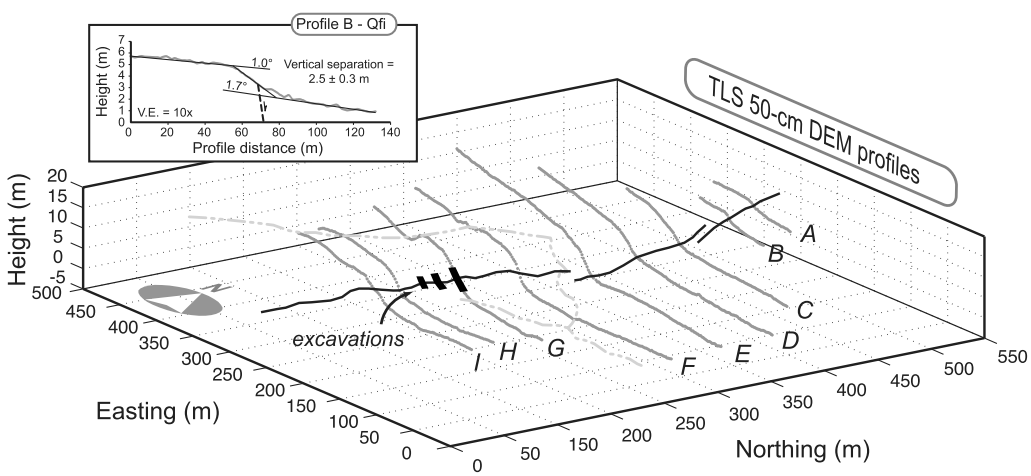

Figure 6. Three-dimensional-perspective image of topographic profiles extracted from our lidar survey. Scarp-normal profiles (gray) show the compound nature of the Sage Flat scarp, while profiles along the fault (black) and transverse ephemeral washes (dashed line) show apparent dextral deflections where they cross the scarp. Inset shows detail of profile B across the Qfi surface north of our trench site.

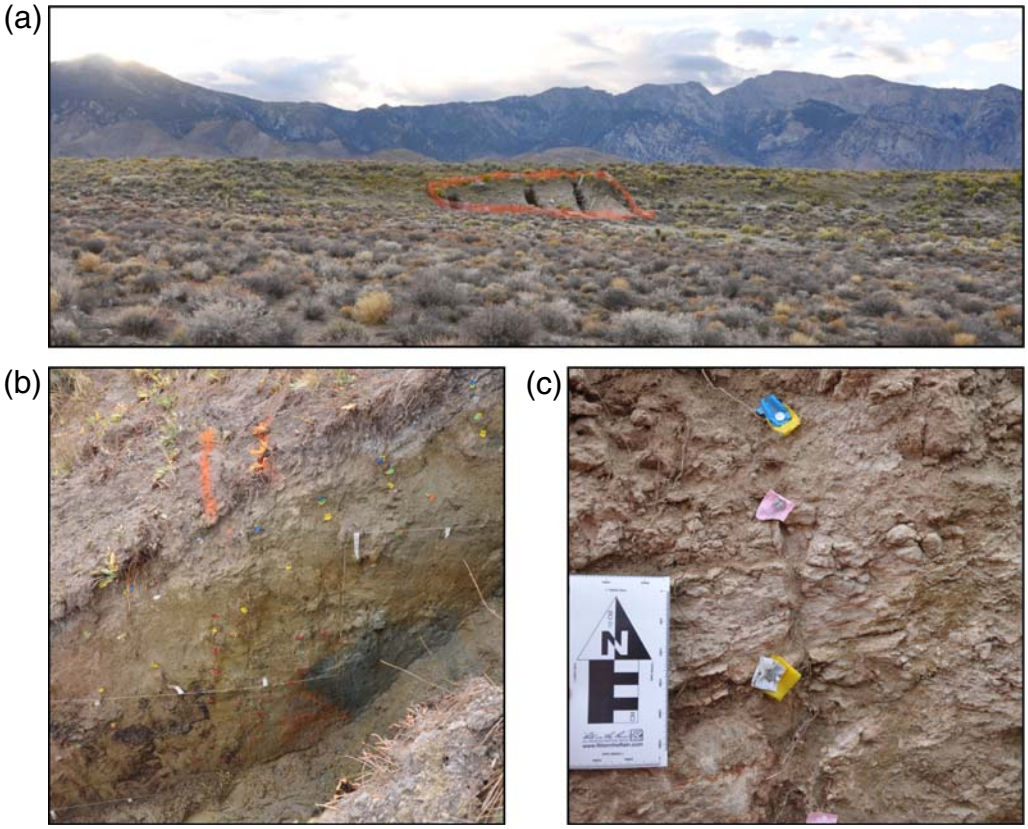

Figure 7. Field photographs of (a) excavations at the Sage Flat site, looking northwest, (b) the southern wall of test pit TP1, and (c) a close up of subvertical fissures filled by young roots and colluvium at the eastern edge of trench T1. The color version of this figure is available only in the electronic edition.

(Fig. 8). Sand of unit 30 is unstratified and very well sorted, suggesting eolian deposition as loess. The upper portion of unit 30 includes a soil profile with some carbonate accumulation (unit 32), weakly developed blocky structure (unit 34), and organic accumulation (unit 36). The basal contact with unit 10 is indistinct and irregular at the decimeter scale. Our trench logs depict this contact as subhorizontal and queried (Fig. 8), although its irregularity may reflect obscuration by subsurface weathering because of saturated groundwater conditions and/or bioturbation.

The youngest stratigraphic deposits exposed in our trenches include two distinct packages of scarp-derived colluvium with soil development (Fig. 8). The oldest of these deposits, unit 40, consists of unstratified brownish yellow silty fine- to medium-grained sand with gravel. Unit 40 is distinguished from the underlying alluvial fan gravels by a lighter color and increased silt component, although the basal contact between these deposits is somewhat gradational. Unit 40 contains cobbles and boulders of similar plutonic and metamorphic rocks as units 10 and 20. The overall geometry of this deposit defines an eastward-thickening wedge (Fig. 8), presumably reflecting erosional stripping and local deposition at the top and bottom the scarp, respectively. Unit 40 includes locally discontinuous soil horizons, possibly attributable to predepositional weathering of the former ground surface. The nature of the lower contact with eolian deposits of unit 30 is obscured by weathering and unclear and is shown as queried on the trench logs (Fig. 8).

Younger colluvial deposits of unit 50 unconformably overlie unit 40 and consist of yellow, fine- to medium-grained silty sand with gravel (Fig. 8). The wedgelike geometry of this deposit similarly suggests deposition as scarp-derived colluvium. Unit 50 is easily distinguished from unit 40 by the general absence of cobbles and boulders and an increased silt component. Stratification within unit 50 is defined by carbonate accumulation (units 52 and 54) and development of soil horizons (units 54 and 56), rather than grain-size sorting. Unit 52 consists of silty fine- to medium-grained sand and is thoroughly cemented with carbonate to form a continuous horizon up to 10-cm thick in trench T1 (Fig. 8). The pedogenic horizon defining unit 52 bifurcates into numerous clay-lined seams that cross into other units and is not exposed to the south in test pit TP1. Unit 54 is cemented with spring carbonate, similar to unit 52, but is less dense and features well-developed platy pedogenic structure. The overlying unit 56 is poorly cemented and features subangular blocky pedogenic structure. The exact nature of the lower contact between colluvial unit 50 and unit 30 is unclear, but the relative abundance of sand and silt in unit 50 is consistent with derivation from the eolian deposits of unit 30.

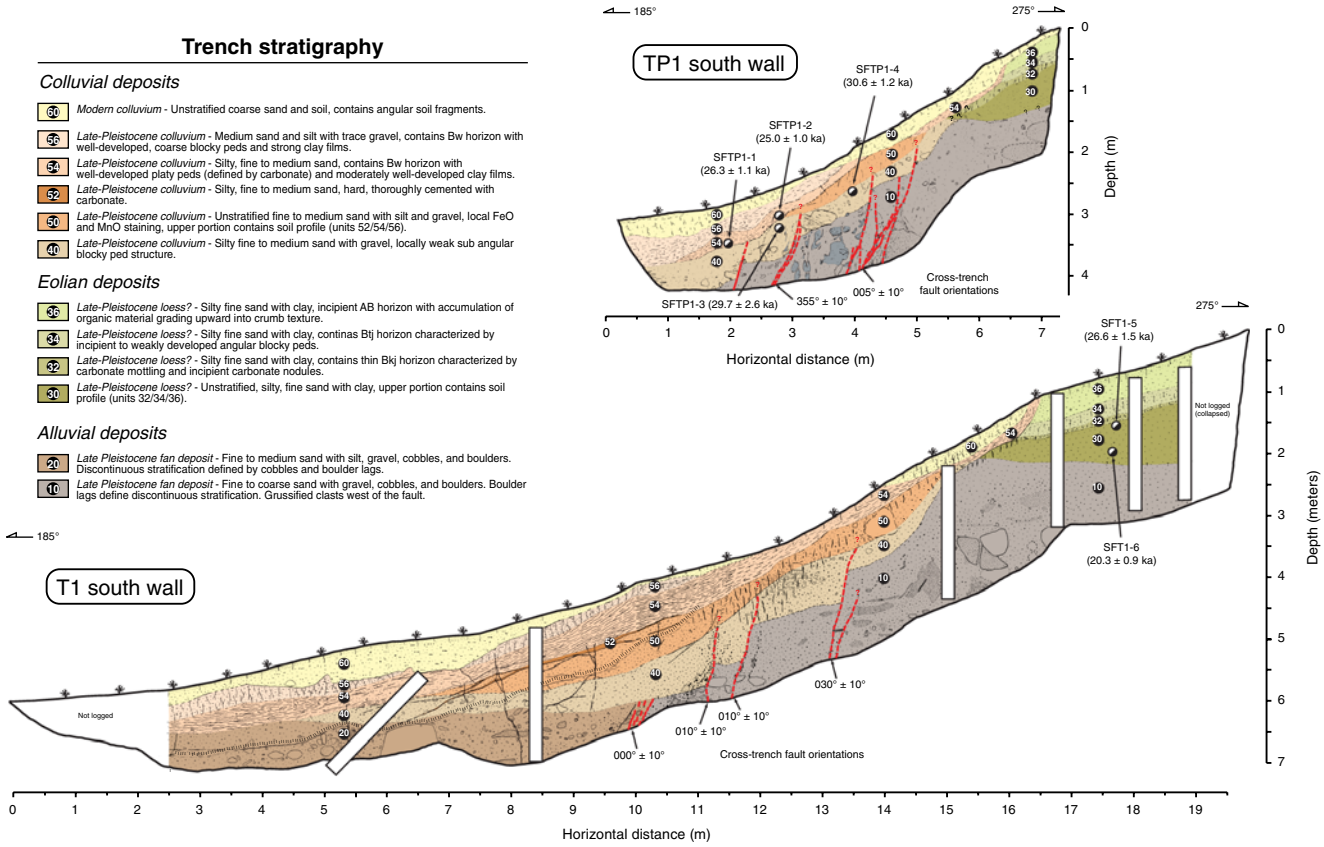

Figure 8. Scaled versions of our interpretive trench logs across the Sage Flat fault. The color version of this figure is available only in the electronic edition.

The modern ground surface is underlain by unit 60, which consists of unstratified medium- to coarse-grained sand with gravel (Fig. 8). This deposit includes angular fragments of carbonate-cemented soil and sediment, representing active raveling of units 36 and 54 from the scarp face.

Faulting and Deformation

Excavations T1 and TP1 exposed a 3-to-4-m-wide zone of faulting midway along the Sage Flat scarp consisting of multiple steeply east-dipping to subvertical fault strands (Fig. 8 and Ⓔ Plates S1 and S2, available in the electronic supplement). Despite extensive weathering and mottling driven by concentration of groundwater along the fault plane, detailed logging of fault exposures from trench T1 and test pit TP1 consistently demonstrate the general characteristics and location of faulting at Sage Flat (Fig. 8). In each trench, a prominent groundwater barrier along the western edge of the fault zone causes pervasive gley mottling at the upper, western end of the scarp, in contrast with brown and reddish hues of manganese- and iron-oxide (MnO and FeO) staining east of the fault (Fig. 7b). Individual fault strands east of this barrier are less well defined but are visible as vertical strings of MnO staining within unit 10 overprinting weathered clay seams with poorly developed shear fabric (Fig. 8). These narrow zones coincide with abrupt vertical steps in the base of unit 40, although faults are indistinct where they continue upward into this colluvial unit. Younger colluvium of unit 50 is apparently undeformed across the Sage Flat fault and represents the oldest unfaulted stratigraphic unit (Fig. 8). Where individual fault planes are visible in both trench walls, measured cross-trench fault orientations yield generally north–south to north-northeast fault strikes between approximately 355° and 030°.

No tilting, warping, or folding of individual stratigraphic layers is apparent in either trench exposure (Fig. 8). The relatively coarse alluvial deposits at the base of each excavation, coupled with pervasive weathering within the fault zone, lend relatively large uncertainties to offset estimations from faulted stratigraphic horizons. Nonetheless, the total vertical separation of the base of colluvial unit 40 summed across individual fault strands in test pit TP1 and trench T1 totals approximately 0.8–1.4 m, respectively, though this is a minimum estimate that does not include displacement along minor fault strands west of the excavations (Fig. 5). Based on the irregularity of the unconformity between this unit and the underlying alluvial gravels, we consider our tape measurements of fault offset in each trench accurate within approximately 50 cm across the width of the fault zone. Total vertical offset of the Qfo fan surface at our trench site totals 7.5 ± 0.7 m, based on profiles extracted from our lidar

Table 1
Results of Optically Stimulated Luminescence (OSL) Analyses for Sage Flat

Sample ID, Location	% Water Content*	K (%)*	U (ppm)†	Th (ppm)†	Cosmic Dose Additions (Gy/ka)††	Total Dose Rate (Gy/ka)	Equivalent Dose (Gy)	n§	Age (ka)‖
SFTP1-1 (TP-1, Unit 54)	15 (38)	1.52 ± 0.02	1.84 ± 0.06	5.80 ± 0.22	0.23 ± 0.02	2.28 ± 0.05	59.9 ± 2.16	17 (20)	26.3 ± 1.1
SFTP1-2 (TP-1, Unit 54)	14 (50)	1.49 ± 0.02	1.71 ± 0.06	6.90 ± 0.21	0.24 ± 0.02	2.21 ± 0.04	55.3 ± 1.94	22 (25)	25.0 ± 1.0
SFTP1-3 (TP-1, Unit 40)	13 (59)	1.48 ± 0.02	2.15 ± 0.06	7.33 ± 0.23	0.23 ± 0.02	2.21 ± 0.04	65.6 ± 5.51	17 (20)	29.7 ± 2.6
SFTP1-4 (TP-1, Unit 40)	20 (35)	1.40 ± 0.02	1.17 ± 0.05	4.32 ± 0.08	0.23 ± 0.02	1.64 ± 0.02	50.1 ± 1.85	23 (25)	30.6 ± 1.2
SFT1-5 (T-1, Unit 30)	20 (44)	1.43 ± 0.02	2.05 ± 0.07	6.91 ± 0.20	0.22 ± 0.02	2.43 ± 0.04	64.6 ± 3.42	17 (20)	26.6 ± 1.5
SFT1-6 (T-1, Unit 30)	22 (40)	2.39 ± 0.04	2.48 ± 0.08	11.4 ± 0.35	0.19 ± 0.01	3.67 ± 0.07	74.5 ± 2.76	19 (20)	20.3 ± 0.9

*Field moisture. Figures in parentheses indicate complete saturation %. Ages calculated using about 25% saturation for Holocene-age samples and 40% saturation for Pleistocene-age samples.

†Analyses obtained using laboratory gamma spectrometry (high resolution Ge detector) and readings are delayed after 21 days of being sealed in the planchet (used for dose rates).

††Cosmic doses and attenuation with depth were calculated using the methods of Prescott and Hutton (1994). Ⓔ See additional material in the electronic supplement for details.

§Number of replicated equivalent dose (De) estimates used to calculate the mean. Figures in parentheses indicate total number of measurements made, including failed runs with unusable data.

‖Dose rate and age for fine-grained 180-90-micron quartz sand. Linear+exponential fit used on equivalent dose, errors to one sigma.

survey (profile G; Fig. 6). This vertical offset corresponds to a dip slip of roughly 7.8 m on a 75° fault plane similar to those exposed in our trenches (Fig. 8). The absence of intact kinematic indicators in each trench or any continuous stratigraphic piercing lines between the two excavations precludes identification or measurement of the lateral component of displacement, if present. Depending on the magnitude of this lateral displacement, the location of our trench site in a slight releasing stepover may serve to amplify the total measured vertical offset (Fig. 5).

A distinct set of subvertical fractures and carbonate, colluvial, and root-filled fissures cuts across stratigraphy at the eastern end of trench T1 (Figs. 7c and 8). With the exception of the uppermost, loose colluvial soil of unit 60, these cracks penetrate each stratigraphic layer without measurable displacement. In places, these fissures cut across weathered boulders of alluvial unit 20 (Ⓔ Plate S1, available in the electronic supplement) and are continuous across the trench to the unlogged northern wall. At their upper termination, these fissures are filled with loose colluvium and roots from the uppermost trench units (Fig. 7c). Fissures and fractures appear disconnected and unrelated in their geometry to the adjacent fault planes (Fig. 8) and possibly reflect deformation related to shaking or lurching of an unbuttressed slope.

Optically Stimulated Luminescence Dating

We used optically stimulated luminescence dating (OSL) in conjunction with the degree of soil profile development to constrain the depositional ages of stratigraphic units in the Sage Flat trenches. A total of six OSL tube samples were collected from eolian unit 30 in trench T1 and colluvial units 40 and 54 in test pit TP1 (Fig. 8). All OSL samples were prepared and analyzed using the single-aliquot regeneration method on quartz at the U.S. Geological Survey Luminescence Dating Laboratory in Denver, Colorado. Table 1 presents the luminescence dating results for each sample, and the detailed parameters and protocol for these OSL analyses are presented in Ⓔ Tables S1 and S2 (available in the electronic supplement). The OSL ages and the associated uncertainties are used to estimate and display the normal kernel density, shown in Figure 9. In the following figures, text, and tables, individual OSL ages are presented and discussed using 1σ uncertainties, while average ages from multiple samples are presented using the associated 2σ errors.

The validity of OSL ages depends upon sufficient exposure to sunlight prior to burial so that each sample is effectively reset to zero and the ages obtained date only the deposition interval of interest (Rhodes, 2011). As such, eolian deposits, such as those collected from the loess unit 30, represent ideal targets for OSL analysis. Although questions surround the suitability of coarse colluvium shed during scarp retreat events, OSL dating has proven effective in paleoseismic efforts to date finer-grained scarp colluvium or buried soil horizons (Forman *et al.*, 2000; Heimsath *et al.*, 2002; Hall and Goble, 2011). As such, we sampled the sandier portion of exposed colluvial wedge deposits, which represent reworked alluvium and loess that originally accumulated along the Sage Flat scarp. Radial plots were constructed for each sample in order to test for the effects of sediment mixing (i.e., bioturbation) or partial bleaching (i.e., incomplete exposure to sunlight prior to burial) as a bias toward younger or older ages, respectively (Ⓔ Figs. S1–S6, available in the electronic supplement).

OSL analysis yields late-Pleistocene ages for all samples from the Sage Flat trench exposures (Fig. 9 and Table 1). With the exception of sample SFTP-6, these ages are consistent with stratigraphic relationships revealed by our trench logging (Fig. 8). The oldest measured OSL ages originate from colluvial unit 40, the buried and deformed colluvial wedge directly overlying alluvial fan gravels of unit 10 (Fig. 8). Analysis of these two samples (SFTP1-3 and SFTP1-4) suggests ages of 29.7 ± 2.6 and 30.6 ± 1.2 ka,

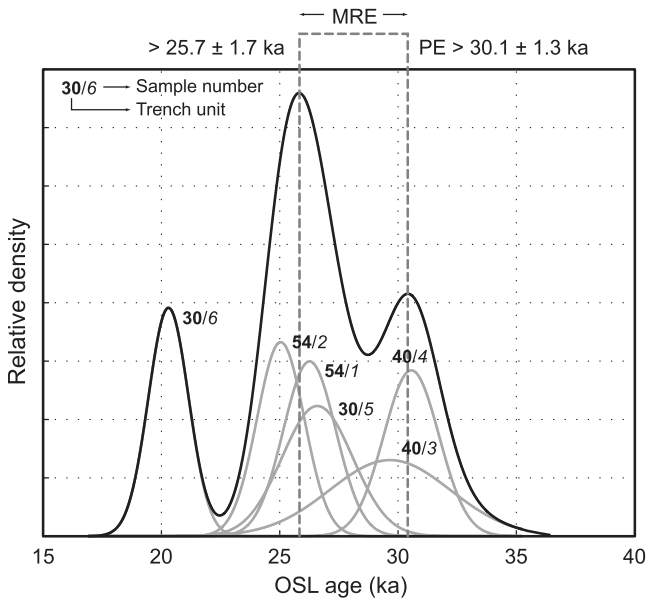

Figure 9. The total results of OSL analyses are presented as individual normal distributions (gray lines) and summed to produce a composite curve (black line). Bold numbers correspond to the sampled unit, and the numbers in italics refer to sample numbers in Table 1.

respectively (Table 1), that contribute to an older peak in the distribution centered at an average age of 30.1 ± 1.3 (2σ) (Fig. 9). Although the radial plots associated with these ages indicate a significant partial bleaching component for sample SFTP1-4, sample SFTP1-3 indicates little bias toward older ages caused by non-reset quartz grains (Ⓔ Figs. S3 and S4, available in the electronic supplement). As such, overall consistency between these two ages lends some credence to the relatively older peak age for these two samples.

OSL dates from the younger, undeformed colluvial wedge (unit 54, Fig. 8) yield consistent ages of 26.3 ± 1.1 and 25.0 ± 1.0 ka for samples SFTP1-1 and SFTP1-2, respectively (Table 1). These ages contribute to a younger, prominent peak in the composite density estimate (Fig. 9) and correspond to an average age of 25.7 ± 1.7 ka (2σ). Although the tails of this peak overlap with the older peak age from colluvial unit 40 (Fig. 9), radial plots for samples SFTP1-1 and SFTP1-2 suggest only minor bias to either younger or older OSL ages (Ⓔ Figs. S1 and S2, available in the electronic supplement).

The two OSL ages calculated for samples collected from eolian sand and silt at the top of trench T1 (unit 30, Fig. 8) indicate relatively young and stratigraphically inconsistent ages. The older of these two dates (sample SFTP1-5) suggests a depositional age of 26.6 ± 1.5 ka, slightly older but in broad agreement with the younger colluvial wedge unit 54 (Table 1 and Fig. 9). The radial plot for sample SFTP1-5 suggests some potential for bias in this age (Ⓔ Fig. S5, available in the electronic supplement), although the relatively finer-grained nature of colluvial unit 54 may suggest derivation from loess within unit 30. The younger age calculated for sample SFT1-6 (20.3 ± 0.9 ka, Table 1) is outlying (Fig. 9) and stratigraphically inconsistent with its location below the older sample SFTP1-5. The radial plot for sample SFT1-6 (Ⓔ Fig. S6, available in the electronic supplement) provides no indication of bias in the calculated OSL age, although we note anomalously high levels of potassium, uranium, and thorium relative to other samples (Table 1), and thus the *in situ* dosimetry might be a possible cause for this age inconsistency. As such, we favor the older of these two dates as representative of the depositional age of eolian unit 30 (26.6 ± 1.5 ka). Although this older age is indistinguishable from the average age calculated for colluvial unit 54 (25.7 ± 1.7 ka, 2σ), a slightly older age for eolian unit 30 is consistent with the observed cross-cutting relationship between these two units (Fig. 8).

Analysis of soil development in trench T1, though limited in ability to resolve absolute ages, is broadly consistent with the OSL dating results. The older colluvial unit 40 (Fig. 8), though highly weathered from the presence of groundwater, contains very few distinct pedogenic features. An exception is a localized area of Bw-horizon development between stations 6.5 and 7.5 m (Ⓔ Plate S1, available in the electronic supplement), which may record colluvial reworking and pedogenesis of highly weathered unit 10 at the main fault scarp in the time period between deposition of units 40 and 54. Colluvial unit 50 exhibits discontinuous carbonate mottling, and units 54 and 56 are pervasively cemented by spring carbonate. Well-developed platy pedogenic structure characterizes colluvial unit 54, and unit 56 exhibits well-developed subangular blocky structure. This degree of soil development is consistent with a relatively prolonged period of pedogenesis (i.e., 25 ka; e.g., Gile *et al.*, 1981; Birkeland *et al.*, 1991; Birkeland, 1999), although the local addition of spring water and carbonate development precludes development of an age estimate based on relative weathering profiles from other landforms in the region.

Discussion

Earthquake Chronology

Taken together, the results of paleoseismic trenching and OSL dating provide evidence and timing for two late-Pleistocene surface rupturing earthquakes on the Sage Flat fault. Deposition of the colluvial unit 50 (Fig. 8) resulted from scarp retreat closely following the most recent earthquake (MRE). Unit 50 contains a substantially higher percentage of finer-grained material than older colluvial deposits (unit 40; Fig. 8), which may reflect incorporation of loess stripped from eolian unit 30 atop the footwall of the Sage Flat fault. The MRE disrupted the older colluvial wedge (unit 40; Fig. 8), resulting in at least ~0.8–1.4 m of vertical separation of its basal contact with the underlying alluvial deposits. An additional, unknown component of lateral displacement may have occurred during this event, causing right-lateral

deflection of ephemeral channels inset within late Pleistocene fans immediately north of the trench site (Fig. 5).

OSL dates from colluvial unit 40 (SFTP1-1 and SFTP1-2; Table 1) provide a minimum age for the MRE of 25.7 ± 1.7 ka (2σ) (Fig. 9). Two distinct interpretations constrain the maximum age of this event. First, OSL ages from colluvial, hanging-wall stratigraphy beneath unit 50 provides a limiting maximum age averaging 30.1 ± 1.3 ka (2σ) (Figs. 8 and 9). Secondly, the older of two ages from footwall unit 30 limits formation of colluvial unit 50 to sometime after 26.6 ± 1.5 ka, although the presence of only one dependable age from unit 30 hampers the reliability of this estimate (Fig. 8). As discussed previously, the finer-grained nature of unit 54 relative to the underlying colluvium of unit 40 may suggest that accumulation of eolian unit 30 occurred between deposition of the two colluvial units. Accordingly, overlap between the preferred OSL age from unit 30 (26.6 ± 1.5 ka, Table 1) and the average age of colluvial unit 54 (25.7 ± 1.7 ka, 2σ) produces the younger composite peak age in Figure 9. This overlap may suggest that the MRE closely followed deposition of eolian unit 30 along the Sage Flat fault.

The penultimate surface-rupturing earthquake on the Sage Flat fault resulted in scarp retreat and formation of an older colluvial wedge (unit 50; Fig. 8). Two OSL ages at the base of this contact limit the timing of this event before 30.1 ± 1.3 ka (2σ) (Fig. 9). Trench exposures at Sage Flat do not constrain the total amount of offset during this earthquake, although we note the presence of a truncated shear zone at the eastern end of trench T1 juxtaposing alluvial deposits of units 10 and 20 (Fig. 8). This shear zone did not rupture during the MRE but might be responsible for some of the total vertical separation of the Qfo surface (~7.5 m, Fig. 6).

A number of subvertical fissures and fractures at the eastern end of trench T1 also imply some degree of surface deformation, possibly linked to seismic shaking on nearby faults. These features cut younger stratigraphic units exposed in our trenches and locally include colluvial fill from the modern ground surface (Fig. 8). Although no slip occurs along this fracture set, their apparently young age leaves open the possibility that they formed in response to strong ground motion during the 1872 Owens Valley earthquake. Linking these features to the 1872 event is purely conjectural, however, given the proximity of the Sage Flat site to numerous other Quaternary-active geologic structures capable of producing surface ruptures and seismic shaking (Fig. 2).

New Fault Slip-Rate Constraints

The combined results of our lidar surveying and OSL dating provide constraints on the maximum vertical slip rate of the Sage Flat fault. If we assume that the penultimate earthquake on this fault produced a similar vertical offset to the MRE (~0.8–1.4 m), we can reasonably speculate that the ~2.5-m scarp cutting the Qfi surface north of the trench site (profile B; Figs. 5 and 6) represents the product of two to three earthquakes. Given the extreme minimum age on the penultimate earthquake here of ~30.1 ± 1.3 ka, this separation translates into a maximum rate of dip slip of 0.09 ± 0.01 mm/yr, assuming a steeply dipping fault plane of ~75°. This calculation utilizes the Monte Carlo method for normal fault scarps outlined by Amos *et al.* (2010) and Rood *et al.* (2011). Although our lidar survey did not capture the laterally deflected stream inset within the young alluvial fan surface (Qfi) just north of profile B (Fig. 4), field measurements indicate ~3 m of dextral offset. This estimate suggests the possibility of comparable magnitudes of both dextral and normal components of offset along the Sage Flat fault.

Implications for the Southern Owens Valley Fault Zone

Our paleoseismic study indicates that the 1872 Owens Valley earthquake did not produce triggered slip on the prominent scarp at Sage Flat. Despite its strong geomorphic expression, steep scarp face, and orientation similar to the Red Ridge fault (Fig. 2), which accommodated triggered slip during the Owens Valley earthquake (Slemmons *et al.*, 2008), our work suggests that the last surface-rupturing earthquake at Sage Flat occurred sometime between ~25.7 and 30.1 ka (Fig. 9). Although somewhat broadly constrained, the antepenultimate earthquake (APE) identified for the Lone Pine strand of the Owens Valley fault at ~15–25 ka (Lubetkin and Clark, 1988; Bacon and Pezzopane, 2007) overlaps with the MRE at Sage Flat. Whether the MRE at Sage Flat occurred as triggered slip during this Owens Valley fault earthquake is unknown, however, given the relatively imprecise bounds on the timing of the Owens Valley APE. In any case, given the preHolocene MRE at Sage Flat and the relatively long return period for Owens Valley earthquakes of ~10 k.y. (Bacon and Pezzopane, 2007), we consider the Sage Flat fault as a geomorphic analog for the prerupture state of Owens Valley fault segments near Lone Pine prior to 1872. Viewing the Sage Flat fault in this context provides a somewhat unique perspective on the potential for large earthquake surface ruptures to occur on somewhat discontinuous fault segments without clear connection to other structures with documented activity.

Trenching at Sage Flat uncovered evidence for recent fractures and subvertical fissures cutting across young stratigraphy, including soil and colluvium at the top of the section underlying the modern ground surface (Fig. 8). Although the exact age of these features is unknown, a possible origin could be as a secondary off-fault deformation caused by nearby seismic shaking. The prevalence of secondary ground deformation in the Haiwee area is consistent with the original observations of ground deformation by Whitney (1872a). We reiterate the point made by Hough and Hutton (2008) that Whitney's observations occurred before the geologic community made the specific connection

between fault slip and earthquakes. Given the locally wet conditions at Sage Flat and presumably surrounding the former Haiwee Meadows, it seems plausible that surface deformation in this area reflects the secondary effects of seismic shaking (e.g., lateral spreading) rather than slip on faults. We also note that both Carver (1969) and Slemmons *et al.* (2008) describe abundant liquefaction-related surface deformation and lateral spreading that occurred associated with the 1872 event within the saturated ground fringing Owens Lake.

The absence of evidence for recent triggered fault slip at the Sage Flat paleoseismic site provides an additional constraint on the southern extent of the 1872 surface rupture. Although it is possible that such slip occurred on other Quaternary faults in the Haiwee area (Fig. 2), the Sage Flat scarp represents the most prominent of these features outside of the modern reservoir (Fig. 7a). As such, the extent of the 1872 rupture spanning from just north of Big Pine near Klondike Lake to the southern end of the Red Ridge fault totals at least 113–120 km (Slemmons *et al.*, 2008; Fig. 1).

Summary of Findings

Paleoseismic trenching at Sage Flat documents stratigraphic and geochronologic evidence for two late-Pleistocene surface-rupturing paleoearthquakes in the Haiwee area. Luminescence dating of sand and silt from two distinct colluvial wedges and from loess deposits capping alluvial fan gravels suggests that the most recent and penultimate earthquakes at Sage Flat occurred between ca. 25.7 and 30.1 ka and before ~30.1 ka, respectively. The most recent event produced a minimum vertical displacement of 0.8–1.4 m. Trenched stratigraphy does not provide conclusive evidence for lateral offset, although dextral deflection of adjacent washes may suggest a comparable component of lateral displacement. Ground-based lidar surveying of deformed alluvial fans, in concert with OSL dating, indicates a maximum dip-slip rate up to ~0.1 mm/yr for the Sage Flat fault, albeit averaged over only two to three earthquakes.

Taken together, our results suggest that triggered slip did not occur on the Sage Flat fault during the 1872 Owens Valley earthquake. Instead, subvertical fissures and fractures cutting across young trench stratigraphy may record secondary deformation associated with seismic shaking during this event. However, we do note, overlap between the timing of the most recent earthquake at Sage Flat and the antepenultimate Owens Valley fault earthquake at Lone Pine (ca. 15–25 ka, Bacon and Pezzopane, 2007). Although our trenching does not exclude the possibility of triggered surface rupture on other faults in the Haiwee area, we suspect that historical descriptions of surface deformation south of the recognized 1872 rupture (Whitney, 1872a) similarly reflect secondary or liquefaction related deformation (e.g., settlement) rather than fault surface rupture.

Consideration of mapping by Duffield and Bacon (1981), Frankel *et al.* (2008), and Jayko (2009) suggests that discontinuous-normal and oblique-normal faults occur north of Lower Cactus Flat. These structures provide a likely kinematic link to the southern Owens Valley fault zone in the northwestern Coso Range. Although no thoroughgoing fault directly links these structures, apparent offset of the eroded margin of a Plio-Quaternary andesite is consistent with dextral displacement along faults north of Cactus Flat. Given the similarity between the orientation and sense of offset for these structures and the Owens Valley fault, we suggest addition to the overall fault length, totaling approximately 140 km from south of Bishop to Lower Cactus Flat. Late Quaternary alluvial deposits in Lower Cactus Flat do not preserve clear evidence for rupture during the 1872 event, thus limiting the southern endpoint of the earthquake surface rupture to the Red Ridge fault (Slemmons *et al.*, 2008). From north of Big Pine to Red Ridge, this surface rupture spans roughly 113–120 km of the total 140-km-long Owens Valley fault.

Exclusion of possible surface faulting associated with the 1872 earthquake at the Sage Flat paleoseismic site confirms that this event ruptured with a relatively high surface displacement (6 ± 2 m; Beanland and Clark, 1994) relative to its length (Hough and Hutton, 2008). Similar displacements were produced during the 1857 and 1906 San Andreas events (e.g., Sieh, 1978) along fault sections two to three times longer than the Owens Valley trace. This result supports the idea that earthquakes along discontinuous, low-slip-rate fault systems that characterize areas of distributed intracontinental deformation (e.g., the eastern California shear zone) might produce stronger ground motions than long-lived, plate-boundary (e.g., San Andreas) structures (cf. Hecker *et al.*, 2010). Given the relatively long return periods for earthquakes such as the Owens Valley event (~10 k.y., Bacon and Pezzopane, 2007), many such faults are understudied and pose an unknown seismic hazard. Although complete evaluation of this hypothesis is beyond the scope of our paper, we note that scarps such as the Sage Flat fault might serve as an analog for the prerupture state of the parts of the Owens Valley fault system. Additional work on this question should focus on the physical basis for anomalously strong ground motions associated with intraplate earthquakes and field documentation of multisegment fault surface ruptures in similar tectonic environments.

Data and Resources

Figure 1 includes fault mapping from the U.S. Geological Survey and California Geological Survey (2006) Quaternary Fault and Fold Database for the United States, available from the USGS website http://earthquakes.usgs.gov/regional/qfaults/ (last accessed September 2012). Sources for other data not collected as part of this study are presented in the reference list.

Acknowledgments

We thank Seth Dee for processing and analyzing the luminescence samples. We also thank Paul Hancock and Anita McProud of Lone Pine,

California, for logistical support during our trenching. Bodo Bookhagen provided use of terrestrial laser scanning survey equipment. Constructive reviews by Steven Bacon, Tim Dawson, and Craig dePolo improved the manuscript. This research was supported by the U.S. Geological Survey, Department of the Interior, under the National Earthquake Hazard Reduction Program (NEHRP), award G09AP00133. The views and conclusions contained in this document are those of the authors and should not be interpreted as necessarily representing the official policies, either expressed or implied, of the U.S. government.

References

American Society for Testing and Materials (ASTM) Standard D2487-00 (2000). Standard Practice for Classification of Soils for Engineering Purposes (Unified Soil Classification System), ASTM International, West Conshohocken, Pennsylvania, doi: 10.1520/D2487-00.

Amos, C. B., K. I. Kelson, D. H. Rood, D. T. Simpson, and R. S. Rose (2010). Late Quaternary slip rate on the Kern Canyon fault at Soda Spring, Tulare County, California, *Lithosphere* **2,** 411–417.

Bacon, S. N., and S. K. Pezzopane (2007). A 25,000-year record of earthquakes on the Owens Valley fault near Lone Pine, California: Implications for recurrence intervals, slip rates, and segmentation models, *Geol. Soc. Am. Bull.* **119,** 823–847.

Bacon, S. N., R. M. Burke, S. K. Pezzopane, and A. S. Jayko (2006). Last glacial maximum and Holocene lake levels of Owens Lake, eastern California, USA, *Quaternary Sci. Rev.* **25,** 1264–1282.

Bacon, S. N., S. K. Pezzopane, and R. M. Burke (2003). Paleoseismology on the Owens Valley fault and Latest Quaternary stratigraphy in Owens Valley near Lone Pine, eastern California, *Final Tech. Rept.*, National Earthquake Hazard Reduction Program, http://earthquake.usgs.gov/research/external/reports/01HQGR0013.pdf (last accessed December 2012).

Bateman, P. C. (1961). Willard D. Johnson and the strike-slip component of fault movement in the Owens Valley, California, earthquake of 1872, *Bull. Seismol. Soc. Am.* **51,** 483–493.

Beanland, S., and M. M. Clark (1994). The Owens Valley fault zone, eastern California, and surface faulting associated with the 1872 earthquake, *U.S. Geol. Surv. Bull. 1982*, 32 pp.

Benn, D. I., L. A. Owen, R. C. Finkel, and S. Clemmens (2006). Pleistocene lake outburst floods and fan formation along the eastern Sierra Nevada, California: Implications for the interpretation of intermontane lacustrine records, *Quaternary Sci. Rev.* **25,** 2729–2748.

Bennett, R. A., B. P. Wernicke, N. A. Niemi, A. M. Friedrich, and J. L. Davis (2003). Contemporary strain rates in the northern Basin and Range Province from GPS data, *Tectonics* **22,** doi: 10.1029/2001TC001355.

Bierman, P. R., A. R. Gillespie, and M. W. Caffee (1995). Cosmogenic ages for earthquake recurrence intervals and debris flow fan deposition, Owens-Valley, California, *Science* **270,** 447–450.

Birkeland, P. W. (1999). *Soils and Geomorphology*, Third Ed., Oxford University Press, New York, 372 pp.

Birkeland, P. W., M. N. Machette, and K. Haller (1991). *Soils as a Tool for Applied Quaternary Geology*, Utah Department of Natural Resources, Geological and Mineral Survey Miscellaneous Publication, 63 pp.

Brossy, C. C., K. I. Kelson, C. B. Amos, J. N. Baldwin, B. Kozlowicz, D. Simpson, M. G. Ticci, A. T. Lutz, O. Kozaci, A. Streig, R. Turner, and R. Rose (2012). Map of the late Quaternary active Kern Canyon and Breckenridge faults, southern Sierra Nevada, California, *Geosphere* **8,** 581–591.

Carver, G. A. (1969). Quaternary tectonism and surface faulting in the Owens Lake basin, California, *MSc. Thesis*, University of Nevada, Reno, Nevada, 113 pp.

dePolo, C. M., D. G. Clark, D. B. Slemmons, and A. R. Ramelli (1991). Historical surface faulting in the Basin and Range Province, Western North-America: Implications for fault segmentation, *J. Struct. Geol.* **13,** 123–136.

Dixon, T. H., E. Norabuena, and L. Hotaling (2003). Paleoseismology and Global Positioning System: Earthquake-cycle effects and geodetic versus geologic fault slip rates in the Eastern California shear zone, *Geology* **31,** 55–58.

Dokka, R. K., and C. J. Travis (1990). Role of the Eastern California shear zone in accommodating Pacific-North-American plate motion, *Geophys. Res. Lett.* **17,** 1323–1326.

Duffield, W. A., and C. R. Bacon (1981). Geologic map of the Coco volcanic field and adjacent areas, Inyo County, California, scale 1:50,000.

Duhnforth, M., A. L. Densmore, S. Ivy-Ochs, P. A. Allen, and P. W. Kubik (2007). Timing and patterns of debris flow deposition on Shepherd and Symmes creek fans, Owens Valley, California, deduced from cosmogenic Be-10, *J. Geophys. Res.* **112,** doi: 10.1029/2006JF000562.

Frankel, K. L., A. F. Glazner, E. Kirby, F. C. Monastero, M. D. Strane, M. E. Oskin, J. R. Unruh, J. D. Walker, S. Anandakrishnan, J. M. Bartley, D. S. Coleman, J. F. Dolan, R. C. Finkel, D. Greene, A. Kylander-Clark, S. Marrero, L. A. Owen, and F. Phillips (2008). Active tectonics of the eastern California shear zone, *Geol. Soc. Am. Field Guides* **11,** 43–81.

Forman, S. L., J. Pierson, and K. Letter (2000). Luminescence geochronology, in *Quaternary Geochronology: Methods and Applications*, J. M. Sowers, J. S. Noller, and W. R. Lettis (Editors), AGU Ref. Shelf, Vol. 4, AGU, Washington, D. C., 157–176.

Gile, L.H., J. W. Hawley, and R. B. Grossman (1981). Soils and geomorphology in the basin and range area of southern New Mexico: Guidebook to the desert project: Memoir, *New Mexico Bureau of Mines and Mineral Resources*, Vol. 39, 222 p.

Hall, S., and R. Goble (2011). New optical ages of the Mescalero sand sheet, southeastern New Mexico, *New Mexico Geology* **33,** 9–16.

Hanks, T. C., and H. Kanamori (1979). Moment magnitude scale, *J. Geophys. Res.* **84,** 2348–2350.

Hecker, S., T. E. Dawson, and D. P. Schwartz (2010). Normal-faulting slip maxima and stress-drop variability: A geological perspective, *Bull. Seismol. Soc. Am.* **100,** 3130–3147.

Heimsath, A. M., J. Chappell, N. A. Spooner, and D. G. Questiaux (2002). Creeping soil, *Geology* **30,** 111–114.

Hill, M. R. (1972). A centennial… The great Owens Valley earthquake of 1972, *Calif. Geol.* **25,** 51–54.

Hobbs, W. H. (1910). The earthquake of 1872 in the Owens Valley, California, *Beit. Geophys.* **10,** 352–385.

Hough, S. E., and K. Hutton (2008). Revisiting the 1872 Owens Valley, California, earthquake, *Bull. Seismol. Soc. Am.* **98,** 931–949.

Jayko, A. S. (2009). Surficial geologic map of the Darwin Hills 30′ × 60′ quadrangle, Inyo County, California, scale 1:100,000.

Kirby, E., S. Anandakrishnan, F. Phillips, and S. Marrero (2008). Late Pleistocene slip rate along the Owens Valley fault, eastern California, *Geophys. Res. Lett.* **35,** doi: 10.1029/2007GL031970.

Le, K., J. Lee, L. A. Owen, and R. Finkel (2007). Late quaternary slip rates along the Sierra Nevada frontal fault zone, California: Slip partitioning across the western margin of the eastern California shear zone-Basin and Range Province, *Geol. Soc. Am. Bull.* **119,** 240–256.

Lee, J., J. Spencer, and L. A. Owen (2001). Holocene slip rates along the Owens Valley Fault, California: Implications for the recent evolution of the Eastern California Shear Zone, *Geology* **29,** 819–822.

Lubetkin, L. K. C., and M. M. Clark (1988). Late Quaternary activity along the Lone Pine fault, eastern California, *Geol. Soc. Am. Bull.* **100,** 755–766.

Oakeshott, G. B., R. W. Greensfelder, and J. E. Kahle (1972). 1872: One hundred years later, *Calif. Geol.* **25,** 55–62.

Perroy, R. L., B. Bookhagen, G. P. Asner, and O. A. Chadwick (2010). Comparison of gully erosion estimates using airborne and ground-based LiDAR on Santa Cruz Island, California, *Geomorphology* **118,** 288–300.

Prescott, J. R., and J. T. Hutton (1994). Cosmic-ray contributions to dose-rates for luminescence and Esr dating: Large depths and long-term time variations, *Radiat. Meas.* **23,** 497–500.

Rhodes, E. J. (2011). Optically stimulated luminescence dating of sediments over the past 200,000 years, *Annu. Rev. Earth Planet. Sci.* **39,** 461–488.

Rockwell, T. K., S. Lindvall, M. Herzberg, D. Murbach, T. Dawson, and G. Berger (2000). Paleoseismology of the Johnson Valley, Kickapoo, and Homestead Valley faults: Clustering of earthquakes in the eastern California shear zone, *Bull. Seismol. Soc. Am.* **90,** 1200–1236.

Rood, D. H., D. W. Burbank, and R. C. Finkel (2011). Spatiotemporal patterns of fault slip rates across the Central Sierra Nevada frontal fault zone, *Earth Planet. Sci. Lett.* **301,** 457–468.

Schoenberger, P. J., D. A. Wysocki, E. C. Benham, and W. D. Broderson (2002). *Field book for Describing and Sampling Soils: Version 2.0*, Natural Resources Conservation Service, National Soil Survey Center, Lincoln, Nebraska, 228 pp.

Sieh, K. E. (1978). Slip along San-Andreas fault associated with Great 1857 earthquake, *Bull. Seismol. Soc. Am.* **68,** 1421–1448.

Slemmons, D. B, E. Vittori, A. S. Jayko, G. A. Carver, and S. N. Bacon (2008). Quaternary fault and lineament map of Owens Valley, Inyo County, eastern California, *Geol. Soc. Am. Field Guides Map and Chart Series* **96,** scale 1:100,000.

Stewart, J. H. (1988). Tectonics of the Walker Lane Belt, western Great Basin Mesozoic and Cenozoic deformation in a zone of shear, in *Metamorphism and Crustal Evolution of the Western US,* W. G. Ernst (Editor), Ruby Volume VII, Prentice Hall, Englewood Cliffs, New Jersey, 685–713.

Stinson, M. C. (1977). Geology of the Haiwee Reservoir 15′ Quadrangle, Inyo County, California, *California Division of Mines and Geology Map Sheet 37*, scale 1:62,500.

Stover, C. W., and J. L. Coffman (1993) Seismicity of the United States 1568–1989 (Revised), *U.S. Geol. Surv. Prof. Paper 1527*, 418 p.

Unruh, J. R., E. Hauksson, F. C. Monastero, R. J. Twiss, and J. C. Lewis (2002). Seismotectonics of the Coso Range-Indian Wells Valley region, California: Transtensional deformation along the southeastern margin of the Sierran microplate, in *Geologic Evolution of the Mojave Desert and Southwestern Basin and Range*, A. F. Glazner, J. D. Walker, and J. M. Bartley (Editors), Geol. Soc. Am. Memoir, Vol. 195, 277–294.

Vittori, E., A. M. Michetti, D. B. Slemmons, and G. Carver (1993). Style of recent surface deformation at the south end of the Owens Valley fault zone, eastern California, *Geol. Soc. Am. Abstr. Programs* **25,** 159.

Wallace, R. E. (1984). Patterns and timing of Late Quaternary faulting in the Great Basin Province and relation to some regional tectonic features, *J. Geophys. Res.* **89,** 5763–5769.

Wells, D. L., and K. J. Coppersmith (1994). New empirical relationships among magnitude, rupture length, rupture width, rupture area, and surface displacement, *Bull. Seismol. Soc. Am.* **84,** 974–1002.

Wesnousky, S. G. (2005). Active faulting in the Walker Lane, *Tectonics* **24,** doi: 10.1029/2004TC001645.

Whipple, K. X., and T. Dunne (1992). The influence of debris-flow rheology on fan morphology, Owens Valley, California, *Geol. Soc. Am. Bull.* **104,** 887–900.

Whitney, J. D. (1872a). The Owens Valley earthquake, in two papers, I—Local details, *Overland Monthly* **9,** 130–140.

Whitney, J. D. (1872b). The Owens Valley earthquake, in two papers, II—General conclusions, *Overland Monthly* **9,** 266–278.

Wills, C. J. (1989). Sierra Nevada fault zone—Haiwee segment, Inyo County, California, *California Division of Mines and Geology Fault Evaluation Report FER-208*, 6 pp.

Zehfuss, P. H., P. R. Bierman, A. R. Gillespie, R. M. Burke, and M. W. Caffee (2001). Slip rates on the Fish Springs fault, Owens Valley, California, deduced from cosmogenic Be-10 and Al-26 and soil development on fan surfaces, *Geol. Soc. Am. Bull.* **113,** 241–255.

Geology Department
Western Washington University
516 High St. MS 9080
Bellingham, Washington 98225
colin.amos@wwu.edu
(C.B.A.)

Lettis Consultants International, Inc.
1981 N. Broadway, Suite 330
Walnut Creek, California 94596
lutz@lettisci.com
unruh@lettisci.com
(A.T.L., J.R.U.)

U.S. Geological Survey
White Mountain Research Center
3000 E. Line St.
Bishop, California 93514
ajayko@usgs.gov
(A.S.J.)

U.S. Geological Survey
Denver Federal Center
Box 25046 MS 974
2nd and Center, Bldg. 15
Denver, Colorado 80225
smahan@usgs.gov
(S.A.M.)

Department of Earth Science
University of California
1006 Webb Hall
Santa Barbara, California 93106
burch@eri.ucsb.edu
(G.B.F.)

Manuscript received 23 January 2012